

Toward the modeling of combustion reactions through discrete element method (DEM) simulations

Received: 22 October 2017 / Accepted: 9 March 2018 / Published online: 17 March 2018 © OWZ 2018

Abstract

In this work, the process of combustion of coal particles under turbulent regime in a high-temperature reaction chamber is modeled through 3D discrete element method (DEM) simulations. By assuming the occurrence of interfacial transport phenomena between the gas and solid phases, one investigates the influence of the physicochemical properties of particles on the rates of heterogeneous chemical reactions, as well as the influence of eddies present in the gas phase on the mass transport of reactants toward the coal particles surface. Moreover, by considering a simplistic chemical mechanism for the combustion process, thermochemical and kinetic parameters obtained from the simulations are employed to discuss some phenomenological aspects of the combustion process. In particular, the observed changes in the mass and volume of coal particles during the gasification and combustion steps are discussed by emphasizing the changes in the chemical structure of the coal. In addition to illustrate how DEM simulations can be used in the modeling of consecutive and parallel chemical reactions, this work also shows how heterogeneous and homogeneous chemical reactions become a source of mass and energy for the gas phase.

Keywords Discrete element method (DEM) simulations \cdot Combustion \cdot Interfacial transport phenomena \cdot Surface chemical reactions

1 Introduction

Since the first experimental observations of surface chemical reactions by the mid-1800s, the study of surface processes has played an important role in industrial processes and development of new materials [23]. The synthesis of ammonia, corrosion of metallic devices, crystal growth, and coal combustion are only a few examples of important chemical processes that occur on the surface of a solid phase. Such pro-

Martina Costa Reis marreis@iqm.unicamp.br

Falah Alobaid falah.alobaid@est.tu-darmstadt.de

Yongqi Wang wang@fdy.tu-darmstadt.de

- ¹ Institute of Chemistry, University of Campinas- UNICAMP, Campinas, São Paulo, Brazil
- Institut Energiesysteme und Energietechnik, Technische Universität Darmstadt, Darmstadt, Germany
- Fachgebiet Strömungsdynamik, Technische Universität Darmstadt, Darmstadt, Germany

cesses differ from the usual homogeneous chemical reactions as the surface reaction rate depends not only on the frequency of collisions between atoms or molecules of reactants on the solid surface, but also on certain properties of the surface, such as the number of active binding sites, temperature, and mobility of reactants.

In general, a surface chemical reaction begins with the mass transport from reactants in the bulk of the fluid phase onto the surface of a solid (step 1). This step is followed by the adsorption of reactants onto the solid surface (step 2), where there occur chemical reactions of the adsorbed reactants (step 3). Finally, this step is succeeded by the desorption of the reaction products from the surface (step 4) and their diffusion toward the bulk of the fluid phase (step 5). Collectively, steps 1 and 5 correspond to the mass transport step, whereas steps 2, 3, and 4 comprise the chemical reaction itself. Therefore, the overall rate of the surface chemical reaction will be limited by the slowest step in the mechanism [20].

The rate of certain surface chemical reactions can be indeed limited by the volume of the pores on the solid surface. This is the case of combustion and gasification reactions of coal, where the molecules of the reactant should not only



diffuse onto the coal surface, but also into its porous structure [24]. Actually, coal is a porous material that contains large amounts of water stored in its pores. Initially, a substantial amount of heat is required in the devolatization step to vaporize the water stored in the pores, as well as to produce char, a solid organic compound largely formed by C(s). Once water has been vaporized, char reacts with $O_2(g)$ to form CO(g) in the burnout step, according to the reaction,

$$C(s) + 1/2 O_2(g) \rightarrow CO(g)$$
. (1)

As char is oxidized by $O_2(g)$, it may also react with $CO_2(g)$ and $H_2O(g)$, according to the following gasification reactions,

$$C(s) + CO_2(g) \rightarrow 2CO(g),$$
 (2)

$$C(s) + H_2O(g) \rightarrow H_2(g) + CO(g)$$
. (3)

In addition, simultaneously with the burnout and gasification steps, $H_2(g)$ and CO(g) may undergo gas-phase chemical reactions to produce $H_2O(g)$ and $CO_2(g)$,

$$H_2(g) + 1/2 O_2(g) \rightarrow H_2O(g),$$
 (4)

$$CO(g) + \frac{1}{2}O_2(g)(g) \to CO_2(g)$$
. (5)

During the above reactions, coal is inevitably consumed, so that the surface area of the particles and the volume of pores change during the course of the reactions. Then, in order to describe the influence of the porous structure in the kinetics of the reaction, the foundations of the Langmuir-Hinshelwood model [14] have been systematically used by numerous researchers to describe the steps of char burnout and gasification [11]. However, one of the shortcomings of this approach is that the real char burnout mechanism is much more complex than that considered in the Langmuir-Hinshelwood model. Moreover, there are also strong evidences [20] that the char burnout rate depends on the surface area of the particles, the coal rank, and the rate of mass transport of $O_2(g)$ into the pores of the coal particles, which is limited by the characteristic lifetime of the eddies present in the mixture.

Therefore, since combustion processes correspond to a set of heterogeneous and homogeneous chemical reactions whose kinetics is strongly influenced by the physical characteristics of the coal particles and by the transport properties of the gas phase, a combined chemical and fluid dynamics approach is essential to understand the most elementary aspects of a combustion process. In view of this, in this work 3D computational fluid dynamic simulations based on the discrete element method (DEM) are performed in order to estimate kinetic and thermochemical parameters for the combustion of coal in a high-temperature reaction chamber. By coupling the equations of solid and gas phases through

source terms, the interfacial transport of mass, linear momentum, and thermal energy between the coal particles and the gas phase is investigated during the combustion process. Although this work only considers the combustion process of coal, the presented methodology may be applied to other chemical systems where there exists a sequence of parallel and competitive reactions occurring under turbulent conditions. The aim of this manuscript is to show how discrete element method simulations may be used to describe interfacial transport phenomena during heterogeneous chemical reactions.

2 Theoretical framework of the discrete element method

2.1 Collision model

For gas-solid mixtures where the volume fraction of the solid phase is larger than 0.004, the number of particles per unit volume of mixture is so high that the frequency of collisions between particles becomes relevant for the thermodynamic behavior of the system [22]. For this reason, it is necessary that the contact forces that arise during the collision between particles are taken into account when one describes the dynamics of solid–gas mixtures. Once these contact forces and other forces that act on the particles have been identified, one may propose a force balance equation for each solid particle of the mixture, so that the trajectory of each particle can be predicted by a step-wise integration of the balance equation over a time interval.

In general, one finds two different collision models in the literature to describe the interactions and contact forces between particles of a solid–gas mixture: a model based on the stochastic approach [19] and a model based on the deterministic approach [8]. In the stochastic approach, a probability of collision for each pair of particles is determined through a Poisson distribution. If the collision between particles occurs, the properties of a certain particle are calculated through the mean values and standard deviations of the properties of the particle itself and its neighboring particles. On the other hand, in the deterministic approach, the collision between particles is determined by solving the equation of motion for every single particle of the solid–gas mixture.

Since the equations of motion and mass conservation for every single particle in the solid–gas mixture need to be solved in the deterministic model, this approach is computationally more expensive than the stochastic one. However, the stochastic approach has faced so many problems that its application has been limited to simpler cases. For example, one of the limitations of the stochastic approach is that it can ensure neither the conservation of kinetic energy, nor the conservation of mass during an elastic collision. Moreover,



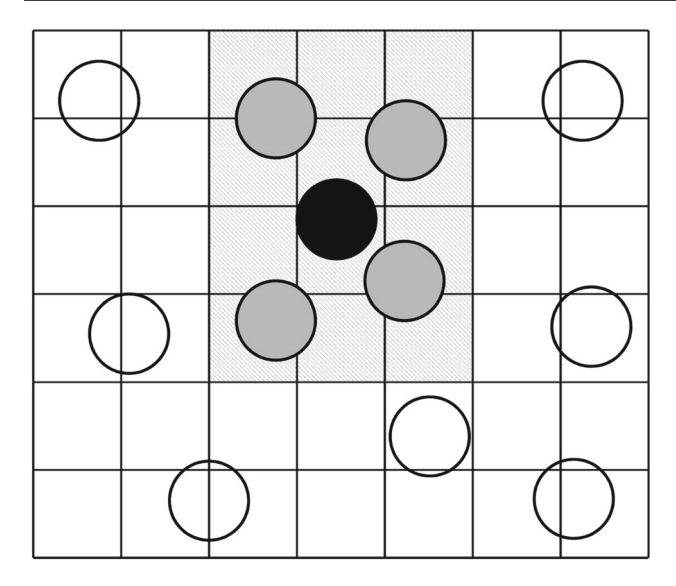


Fig. 1 Collision mesh considered in discrete phase simulations. The black sphere corresponds to the parcel of interest in a time step. Only those parcels in the hatched area are taken into account in the calculations for the contact force. The white spheres represent those parcels that do not interact with the parcel of interest

it does not offer the possibility of taking into account multiple collisions between particles simultaneously. Therefore, in view of this, the deterministic approach becomes preferable, despite the high computational cost.

A way of dealing with the large number of particles in the deterministic approach is to group the similar particles into sets called of parcels, which can be defined in terms of the diameter or mass of particles. Then, the position and velocity of a particular parcel is determined by the trajectory of a single representative particle of the parcel. For this purpose, one assumes that the mass of the representative particle is equal to the mass of parcel m_{parcel} , and the volume of the parcel V_{parcel} is equal to the ratio between m_{parcel} and the particle mass density ρ_i .

According to the deterministic approach [9], each particle in the multiphase system is tested at each time *t* for possible collisions with other particles and with walls of the vessel. A collision will occur if particles move toward each other, and if the distance between the center-points of two particles is smaller than the sum of the respective radii. However, for this purpose, only the closest particles to the investigated particle will be considered. Particles that are far from the influence radius of the investigated particle are neglected since the chance of a possible collision is negligibly small (Fig. 1). During the collision, particles may overlap each other or even penetrate into the wall, so that the resulting contact force in this process can be estimated from the Voigt–Kelvin model.

The Voigt–Kelvin model is a mechanical model that describes how the interactions between particles evolve over time during a collision [7]. In order to describe the inter-

action between particles, Voigt and Kelvin proposed to represent the contact force in terms of a spring, dashpot, and damper connected in parallel. In this model, the spring describes the perfectly elastic collision, whereas the dashpot and the damper elements account for the time-dependent deformation and the dissipation of energy during an inelastic collision, respectively. Then, basically, the contact force on a particle i is obtained by adding all its normal \boldsymbol{F}_{ij}^n and tangential \boldsymbol{F}_{ij}^t components [13],

$$F_{i}^{c} = \sum_{i=1}^{N} \left(F_{ij}^{n} + F_{ij}^{t} \right), \tag{6}$$

where *N* stands for the number of contacts for the particle *i*. Each component of the contact force may be now determined by considering the elements of a spring-dashpot-damper system. For example, the normal component of the contact force between the particles *i* and *j* is given by the summation of elastic and damping forces,

$$\boldsymbol{F}_{ij}^{n} = -k^{n} \left(\delta^{n}\right)^{a} \mathbf{n}_{ij} - \eta^{n} \mathbf{u}_{ij}^{n}, \tag{7}$$

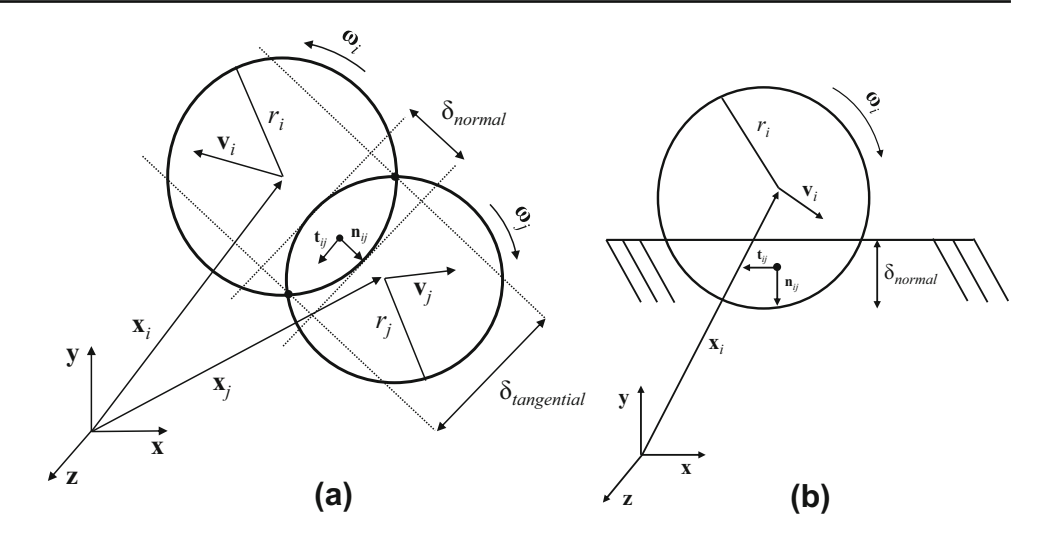
where k^n is the normal stiffness constant, η^n denotes the normal damping coefficient, which depends on the coefficient of restitution in the normal direction, δ^n is the normal displacement defined by $\delta^n = r_i + r_j - |\mathbf{r}_{ij}|$, such that \mathbf{r}_{ij} is the position vector and r_i is the radius of a particle, a is a constant related to a specific spring contact model, \mathbf{n}_{ij} is the normal unit vector, and \mathbf{u}_{ij}^n is the relative velocity in the normal direction (Fig. 2). Here, the vector \mathbf{n}_{ij} is related to the position vector by $\mathbf{r}_{ij} = |\mathbf{r}_{ij}| \mathbf{n}_{ij}$, whereas \mathbf{u}_{ij}^n is defined as $\mathbf{u}_{ij}^n = \left| \mathbf{u}_{ij}^n \right| \mathbf{n}_{ij}$. In general, for calculations of F_i^c , the Hookean approach is satisfactory for most applications. However, for cases where changes in the geometrical and physical properties of the colliding particles are expected, a nonlinear approach for the normal displacement is recommended. In this case, the shear modulus and the Poisson ratio should be taken into account in the determination of the normal stiffness constant.

On the other hand, the tangential component of the contact force is determined on basis of a spring-damper-slider system. Basically, the tangential component of the contact force may be either a static force or a sliding force,

$$\boldsymbol{F}_{ij}^{t} = \begin{cases} \underbrace{-k^{t} \left(\boldsymbol{\delta}^{t}\right)^{a} - \eta^{t} \mathbf{u}_{ij}^{t}}_{\boldsymbol{F}_{\text{static}}^{t}}, & \left| \boldsymbol{F}_{\text{static}}^{t} \right| \leq \left| \boldsymbol{F}_{\text{sliding}}^{t} \right| \\ \underbrace{-\mu \left| \boldsymbol{F}_{ij}^{n} \right| \mathbf{t}_{ij}}_{\boldsymbol{F}_{\text{sliding}}^{t}}, & \left| \boldsymbol{F}_{\text{static}}^{t} \right| > \left| \boldsymbol{F}_{\text{sliding}}^{t} \right| \end{cases}$$
(8)



Fig. 2 Colliding systems considered in discrete element method simulations: (a) particle–particle collisions and (b) particle–wall collisions. The determination of the contact forces during particle–wall collisions may be performed in a similar way as the calculation of the contact forces during particle–particle collisions, if the wall is assumed to be a particle of infinite radius and the translational and rotational velocities are null



where k^t is the tangential stiffness coefficient, η^t is the tangential damping coefficient, μ is the dynamic friction coefficient, δ^t is the tangential penetration depth vector, \mathbf{u}_{ij}^t is the tangential relative velocity given by $\mathbf{u}_{ij}^t = \left|\mathbf{u}_{ij}^t\right|\mathbf{t}_{ij}$, and \mathbf{t}_{ij} is the tangential unit vector given by $\mathbf{u}_{ij}^t = \mathbf{t}_{ij}\left|\mathbf{u}_{ij}^t\right|$. Unlike the normal displacement, δ^t cannot be explicitly calculated from the positions of each particle. However, it can be estimated by considering the integration of the relative tangential velocity at the contact point between two colliding particles over the particle time step,

$$\delta^t = \int_{t_0}^t \left| \mathbf{u}_{ij}^t \right| \mathrm{d}t. \tag{9}$$

Once the normal and tangential components of the contact force have been calculated, one may determine the moment of the contact force. The moment of the contact force on the particle i is given by

$$\boldsymbol{M}_{i} = \sum_{j=1}^{N} r_{i} \boldsymbol{F}_{ij}^{t} \times \mathbf{n}_{ij}, \tag{10}$$

which depends only on the tangential component of the contact force F_{ij}^t . While the tangential component of the contact force is responsible for inducing a rotational motion in the particle, the normal component of the contact force describes the rolling resistance between the colliding particles. For rigid particles whose contact is restricted to a point and for colliding particles whose penetration depth is small, the normal component of the contact force may be neglected.

2.2 Balance of force on the particles

One of the main characteristics of the discrete element method simulations is that the trajectories of particles can be determined throughout a process, as long as one knows the forces and moments of force that act on the particles. Basically, the translational motion of a particle can be determined from Newton's second law of motion, whereas the rotational motion can be estimated from the balance of angular momentum of the particle [1,10]. For the translational motion, one writes

$$m_i \frac{\mathrm{d}\mathbf{v}_i}{\mathrm{d}t} = \mathbf{F}_i^v + \mathbf{F}_i^f + \mathbf{F}_i^c + \mathbf{F}_i^a, \tag{11}$$

where m_i is the mass of a particle i, \mathbf{v}_i is its translational velocity, \mathbf{F}_i^v represents the body force that acts on the particle, \mathbf{F}_i^f represents the force that appears due to the interaction between the fluid phase and the particles, \mathbf{F}_i^c represents the contact force previously discussed, and \mathbf{F}_i^a represents the adhesive force.

The body force F_i^v includes those forces imposed by sources outside the system, such as the gravitational field, and electromagnetic field. While the body forces act throughout the body regardless of its velocity, the forces represented by F_i^f are closely related to the relative velocities of the fluid and solid phases and to the complex structure of the interactions between particles and fluid. In order to describe the forces F_i^f , one assumes that the net motion of a particle in a fluid is given by a combination of independent motions, namely: (a) the particle moves in an isotropic flow field with a constant velocity, (b) the particle accelerates in an isotropic flow field with a constant velocity, and (d) the particle rotates in an isotropic flow field with a constant angular velocity.

Each of the motions above described is responsible for a different force acting on the particle. For example, the force resulting from the motion (a) corresponds to a resistance force, also known as drag force, which arises from an unbalanced pressure distribution on the particle surface. The force that emerges from the motion (b) is also a resistance force.



Whenever a particle accelerates in a fluid, the fluid surrounding the particle accelerates, so that its volume is changed too. This motion creates additional resistance forces that are referred to as virtual mass force and Basset force. In addition to these resistance forces, a particle can also be under the influence of forces that stem from gradients present in an anisotropic fluid, such as in the motion (c). This is the case of the pressure gradient force, Saffman force, thermophoretic force, to name only a few examples. In turn, the rotational motion (d) is related to the Magnus effect that a spinning particle can experience, whenever an irregular pressure distribution is formed on the particle surface.

Finally, the translational motion of a particle can be changed by short-range forces that act between particles, which are represented by the contact forces and the adhesive forces. Likewise the contact forces, the adhesive forces strongly depend on the particle diameter, particle density, and some physicochemical properties. However, they tend to become more relevant as the particle diameter decreases. This is the case of the van der Waals forces, ion-induced dipole forces, and ion-dipole forces, which are responsible for determining interactions between molecules, atoms or ions. For dispersions whose particles present diameter larger than 1.0 µm, adhesive forces can be neglected.

The description of the rotational motion of particles in a fluid is straightforward, if one supposes that the penetration depth observed during a collision between spherical particles is very small. In this case, the rotational motion is only due to the moment of the tangential contact force, and the balance of angular momentum is given by

$$I_i \frac{\mathrm{d}\mathbf{w}_i}{\mathrm{d}t} = \sum_{j=1}^N r_i \mathbf{F}_{ij}^t \times \mathbf{n}_{ij},\tag{12}$$

where I_i is the moment of inertia, and \mathbf{w}_i is the angular velocity of the particle i.

2.3 Mass and energy transfers between the fluid and solid phases

Changes in the mass, linear momentum, and thermal energy of the particles are somehow related to changes in the properties of the fluid phase. A chemical reaction may occur on the surface of particles, so that gases are released to the fluid phase and, consequently, the mass of the fluid phase increases. Similarly, a particle may accelerate in a solid–gas mixture, leading to the acceleration of the fluid surrounding the particles. These examples describe only a few phenomena in which quantities of the particulate phase are coupled to parameters of the fluid phase in a multiphase system.

As a matter of fact, by postulating balances of mass and thermal energy for each solid particle of the mixture, one may follow the changes in the mass and thermal energy of a particle while it performs a certain motion. However, since changes in the mass, linear momentum, and thermal energy of a particle are related to changes in the dynamics of the gas phase, one should also consider the balances of mass, linear momentum, and energy of the gas phase. For this purpose, one regards the fluid phase as a continuous body whose dynamics is given by the usual balance equations of continuum mechanics [21],

Balance of mass

$$\rho_f \frac{\partial \alpha_f}{\partial t} + \rho_f \operatorname{div} \left(\alpha_f \mathbf{v}_f \right) - \lambda_f - a_{fs} c_f = 0, \tag{13}$$

Balance of linear momentum

$$\rho_{f} \frac{\partial \alpha_{f} \mathbf{v}_{f}}{\partial t} + \rho_{f} \operatorname{div} \left(\alpha_{f} \mathbf{v}_{f} \otimes \mathbf{v}_{f} \right) - \operatorname{div} \left(\mathbf{T}_{f} \right) - \rho_{f} \alpha_{f} \mathbf{g}$$
$$-\beta_{fs} \left[\sum_{i=1}^{n} \left(\mathbf{v}_{i} - \mathbf{v}_{f} \right) \right] + a_{fs} c_{f} \mathbf{v}_{f} = \mathbf{0}, \tag{14}$$

Balance of enthalpy

$$\rho_f \frac{\partial \alpha_f \gamma_f}{\partial t} + \rho_f \operatorname{div} \left(\alpha_f \gamma_f \mathbf{v}_f + \mathbf{h}_f \right) - \mathbf{T}_f \cdot \nabla \mathbf{v}_f - \rho_f \alpha_f r - a_{fs} q_f - a_{fs} c_f \gamma_f = 0,$$
(15)

where ρ_f is the fluid mass density, α_f and α_s , respectively, are the fluid volume fraction and the solid volume fraction, such that $\alpha_f + \alpha_s = 1$, \mathbf{v}_f is the partial velocity of the fluid phase, λ_f is the mass source associated with a homogeneous chemical reaction, a_{fs} is the particle–fluid interfacial area per unit volume of mixture, c_f is the interfacial mass transfer rate, \mathbf{T}_f is the stress tensor, \mathbf{g} is the gravitational field, β_{fs} is the interaction momentum transfer coefficient, which may be defined in terms of the drag coefficient, particle Reynolds number, particle diameter, and fluid dynamic viscosity, n is the number of particles per unit mixture volume, γ_f is the enthalpy density of the fluid phase, \mathbf{h}_f is the heat flux, r is the enthalpy source density, and q_f is the interfacial enthalpy transfer rate.

Clearly, some quantities that appear in the above balance equations depend on the characteristics of the fluid and how the fluid phase interacts with the solid phase. Such properties are called constitutive properties and they are given by specific material laws that characterize the thermomechanical responses of a particular system. While postulation of constitutive laws for the interfacial area, stress tensor, drag coefficient and heat flux is straightforward, postulation of constitutive laws for the interfacial mass transfer rate and interfacial enthalpy transfer rate is troublesome. The main reason for this is due to the fact that one should specify constitutive laws for interfacial transfers based on physicochemical



parameters whose values usually are not available, as well as on chemical mechanisms that are not always well-known.

In order to make the postulation of constitutive laws easier for the interfacial mass transfer rate, one initially regards the combustion process as a sequence of reactions that consist of the devolatization step, reactions on the surface particle, and homogeneous reactions in the fluid phase [4]. Moreover, one assumes that all coal particles are composed of a homogeneous complex organic material that after the devolatization step forms char. Equation (16) describes the changes in the particles mass during the devolatization and burnout steps,

$$\frac{dm_{i}}{dt} = -k_{0}^{\text{dev}} f_{v,0} m_{i,0} - \sum_{r=1}^{N_{r}} \mathcal{R}_{r,i}
\mathcal{R}_{r,i} = a_{i} \eta_{r} \alpha_{w,i} k_{r,i}
k_{r,i} = k_{r}^{0} \left(p - \frac{k_{r,i}}{D_{0,r}} \right)^{l_{r}},$$
(16)

where k_0^{dev} is a constant rate given by the Arrhenius equation whose unit is \mathbf{s}^{-1} , $f_{v,0}$ is the initial fraction of volatile species present in the coal particles, $m_{i,0}$ is the initial mass of the coal particles, N_r encompasses all chemical reactions that occur on the surface of a particle i, $\mathcal{R}_{r,i}$ is the consumption rate of combustibles on a particle i whose unit is $\mathbf{kg}\,\mathbf{s}^{-1}$, a_i is the surface area of a particle i, η_r is the effectiveness factor related to a reaction r, $\alpha_{w,i}$ is the fraction of combustibles present in the particle i, $k_{r,i}$ is the reaction rate per unit area of a particle i whose unit is $\mathbf{kg}\,\mathbf{m}^2\mathbf{s}^{-1}$, k_r^0 is a reaction constant given by the Arrhenius equation whose unit is \mathbf{s}^{-1} , p is the hydrostatic pressure shared by all phases in the solid–gas mixture, $D_{0,r}$ is a parameter that accounts for the diffusion rate of gaseous reactants into the pores during a reaction r, and l_r is the apparent order of reaction r.

During the devolatization step, volatile components are removed from the coal matrix, and the mass of particles is accordingly changed. The rate with which volatile species are removed from the coal matrix is given by the first term on the right-hand side of Eq. (16). Once the volatile species enter into the fluid phase, the combustible fraction of the coal is consumed and residual ash accumulates on the particles. In this case, changes in the particle mass are given by the second term on the right-hand side of Eq. (16).

The last step of a combustion process is a sequence of chemical reactions that occur in the gas phase. Unlike the previous steps, these reactions are homogeneous and, therefore, the particle surface plays no role in the kinetics of the reaction. For the sake of simplicity, one assumes that the gas phase is actually a mixture of different gaseous chemical species. Thus, by neglecting the term for heterogeneous chemical reactions, Eq. (13) takes the form,

$$\frac{\partial \rho_f^{\nu} \alpha_f^{\nu}}{\partial t} + \operatorname{div} \left(\rho_f^{\nu} \alpha_f^{\nu} \mathbf{v}_f \right) + \operatorname{div} \left(\mathbf{j}_f^{\nu} \right) - \lambda_f^{\nu} = 0, \tag{17}$$



where ρ_f^v is the mass density of a component v in the fluid phase, α_f^v is the volume fraction of a component v, \mathbf{j}_f^v is the diffusive flux of a component v, and λ_f^v is the mass source associated with a homogeneous chemical reaction for a component v, such that $\alpha_f = \sum_{v=1}^{N_v} \alpha_f^v$, $\alpha_f \rho_f \mathbf{v}_f = \sum_{v=1}^{N_v} \alpha_f^v \rho_f^v \mathbf{v}_f^v$, $\lambda_f = \sum_{v=1}^{N_v} \lambda_f^v$, and N_v accounts for all chemical species present in the gas phase. Usually, the mass source for a component v due to a homogeneous reaction is evaluated by a modified version of the Arrhenius equation,

$$\lambda_f^v = \sum_{r=1}^{N_r} k_{r,v} \qquad k_{r,v} = A_r T^b \exp\left(-\frac{E_r^a}{RT}\right),\tag{18}$$

where A_r is the pre-exponential factor, T is the temperature on the absolute scale, which is regarded as approximately equal to the temperature of the fluid phase θ_f , b is the temperature exponent, E_r^a is the activation energy of reaction r, and R is the molar gas constant. For those reactions that occur in laminar flow regimes, Eq. (18) provides satisfactory results. However, when the reacting flow becomes turbulent, some physical quantities experience spatial and temporal fluctuations that are not taken into account in Eq. (18). In this case, the modified version of the Arrhenius equation should be dropped in favor of a more adequate equation, such as that provided by the eddy dissipation model .

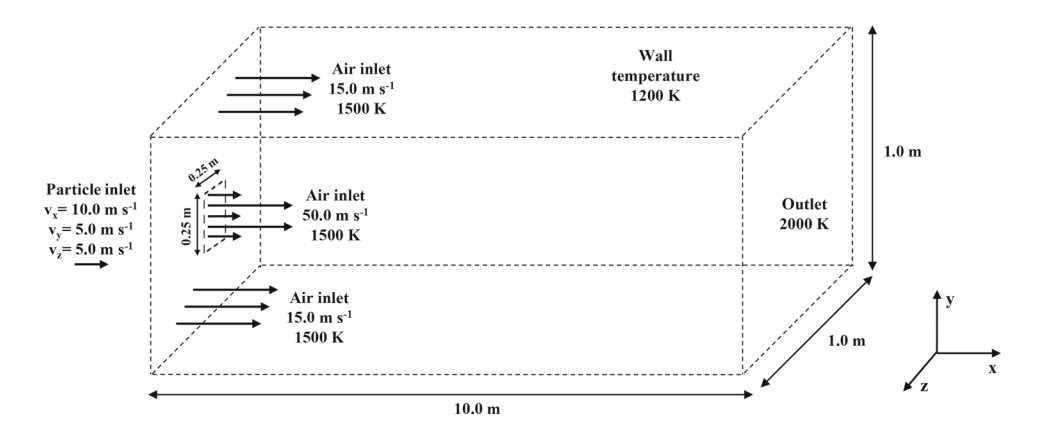
The eddy dissipation model proposed by Magnussen and Hjertager [16,17] assumes that the reaction rate is limited by the turbulent mixing of reactants. In other terms, a chemical reaction will not occur until the eddies in which the reactants are found are dissipated and mixing of reactants is allowed. Since the time necessary for eddy dissipation is determined by the ratio between the turbulent kinetic energy k and the rate of dissipation of the turbulent kinetic energy ϵ , it is natural that the constant rate of a reaction in a turbulent medium is defined as.

$$k_{r,v} = \mathcal{A}v'_{r,v}M_v\left(\frac{\epsilon}{k}\right)\rho_f \min\left(\frac{\alpha_f^{\mathcal{R}}}{v'_{r,\mathcal{R}}M_{\mathcal{R}}}, \frac{\mathcal{B}\sum_{p=1}^P \alpha_f^p}{\sum_{v=1}^{N_v} v'_{r,v}M_v}\right),\tag{19}$$

where \mathcal{A} and \mathcal{B} are empirical parameters, respectively, equal to 4.0 and 0.5, $v'_{r,v}$ is the stoichiometric coefficient of a reactant v in the reaction r, M_v is the molecular weight of the reactant v, $\alpha_f^{\mathcal{R}}$ is the volume fraction of a specific reactant \mathcal{R} , $v'_{r,\mathcal{R}}$ is the stoichiometric coefficient of reactant \mathcal{R} in the reaction r, $M_{\mathcal{R}}$ is the molecular weight of reactant \mathcal{R} , and α_f^p is the volume fraction of a product p in the gas phase. Likewise, in turbulent flows, the constitutive equation for the diffusive flux is usually given by

$$\mathbf{j}_{f}^{v} = -\left(\rho_{f}^{v} D_{m}^{v} + \frac{\mu_{t}}{\operatorname{Sc}_{t}}\right) \nabla \alpha_{f}^{v} - D_{\theta_{f}}^{v} \frac{\nabla \theta_{f}}{\theta_{f}},\tag{20}$$

Fig. 3 Computational domain employed in the simulation



where D_m^v is the diffusion coefficient, μ_t is the turbulent viscosity, Sc_t is the turbulent Schmidt number, and $D_{\theta_f}^v$ is the thermal conductivity coefficient.

While the mass source for homogeneous chemical reactions in the gas phase may be directly obtained from Eq. (19), the interfacial mass transfer for the gas phase needs to be obtained from the mass balance of each coal particle of the mixture. By adding up Eq. (16) over all particles of the mixture, the terms on the right-hand side of the summation result in the interfacial mass transfer rate for the solid phase c_s . Then, since c_s is related to c_f by $a_{fs}c_s = -a_{fs}c_f$, it follows that the interfacial mass transfer rate for the fluid phase is

$$a_{fs}c_f = \sum_{i=1}^n k_0^{\text{dev}} f_{v,0} m_{i,0} + \sum_{i=1}^n \sum_{r=1}^{N_r} \mathcal{R}_{r,i}.$$
 (21)

To close the system of equations for the fluid phase, one should also postulate a constitutive law for the interfacial enthalpy transfer rate q_f . During the devolatization and the combustion steps, the balance of thermal energy of a particle i is given by,

$$m_i c \frac{\mathrm{d}\theta_i}{\mathrm{d}t} = \sigma a_i \left(\theta_f - \theta_i\right) - L \frac{\mathrm{d}m_i}{\mathrm{d}t} - \beta H^r \frac{\mathrm{d}m_i}{\mathrm{d}t},\tag{22}$$

where c is the specific heat of the coal, θ_i is the temperature of a particle i, σ is the convective heat transfer coefficient, L is the specific latent heat of the coal, β is the fraction of heat absorbed by the particle itself, and H^r accounts for the heat released by the coal combustion reaction. Hence, by adding up Eq. (22) over all particles i, the interfacial enthalpy transfer rate is given by

$$a_{fs}q_f = -\sum_{i=1}^n \left[\sigma a_i \left(\theta_f - \theta_i \right) - L \frac{\mathrm{d}m_i}{\mathrm{d}t} - \beta H^r \frac{\mathrm{d}m_i}{\mathrm{d}t} \right]. \tag{23}$$

In general, the fraction of heat absorbed by a particle depends on how the combustion step proceeds. If the coal undergoes an incomplete combustion, $\beta=1.0$ and all heat released during the char burnout process is absorbed by the particle. On the other hand, if coal undergoes a complete combustion, some studies indicated that only 30% of the released heat can be absorbed by a particle [6].

3 3D discrete element method simulation for the combustion process

Three-dimensional discrete element method simulations are performed for the combustion of medium-volatile spherical coal particles whose diameters change from 70 to 200 μ m, according to a Rosin–Rammler distribution with spread parameter equal to 4.52. For this purpose, one considers that 145 coal particle parcels of diameter of 1.0 mm at 300 K are injected at a rate of 0.1 kg s⁻¹ into a chamber of dimensions $10.0 \, \text{m} \times 1.0 \, \text{m} \times 1.0 \, \text{m}$ whose walls are initially thermostatized at $1200 \, \text{K}$. During the combustion process, a mixture of gaseous species (77% $N_2(g)$, 23% $O_2(g)$) at 1500 K continuously flows into the chamber through the two inlets under the turbulent regime (Re ≈ 100000), according to specifications given in Fig. 3 [2].

In order to simulate the combustion of the coal particles, Eqs. (13), (14), (15), and (17) are numerically solved together with the balances of mass (Eq. 16), linear momentum (Eq. 11), and energy (Eq. 22) of each particle for the variables $\mathbf{v}_f(\mathbf{x},t)$, $\gamma_f(\mathbf{x},t)$, $\alpha_f(\mathbf{x},t)$, $m_i(t)$, $m_i(t)$, $m_i(t)$, and $m_f^v(\mathbf{x},t)$, by considering the coal properties given in Table 1 and the simplistic chemical mechanism given in Table 2. During the simulation, the mass density and the specific heat of the gaseous mixture are, respectively, determined by the incompressible-ideal-gas law and the mixing law, and the thermal conductivity and the viscosity of the gas phase are defined by the ideal-gas mixing law. Moreover, coal particles are assumed to behave as elastic materials with a normal stiffness constant of $100 \, \mathrm{N} \, \mathrm{m}^{-1}$ and a tangential damping



Table 1 Physicochemical properties of the coal particles

Physical property	Value
Density	$1300 \mathrm{kg} \mathrm{m}^{-3}$
Specific heat	$1000\mathrm{Jkg^{-1}K^{-1}}$
Latent heat	0
Vaporization temperature	400 K
Fraction of volatile component	28%
Binary diffusivity	$5.0 \times 10^{-4} \mathrm{m}^{-2}\mathrm{s}$
Swelling coefficient	2
Combustible fraction	64%
Fraction of reaction heat absorbed	30%
Devolatization constant	$50 \mathrm{s}^{-1}$

coefficient equal to $0.5\,\mathrm{N}\,\mathrm{m}^{-1}$. For the sake of simplicity, coal particles do not undergo rotational motion, and they are not subject to adhesive forces, such as van der Waals interactions. To complete the formulation of the problem, one assumes that both solid and liquid phases have zero velocity in relation to the stationary walls of the vessel (no-slip condition).

The simulation is performed through the commercial computational fluid dynamic software ANSYS/Fluent 16.2 [3], by using a coupled scheme and the realizable $k-\epsilon$ turbulence model (Table 3) [12]. A mesh of 47,685 hexahedral elements of size length of 6.0 cm is built on a parallelepiped of $10.0 \, \mathrm{m} \times 1.0 \, \mathrm{m} \times 1.0 \, \mathrm{m}$, according to the mapped face meshing method. In addition, a second-order upwind scheme is employed for spatial discretizations of equations of momentum, turbulent kinetic energy, turbulent dissipation rate, energy and volume fraction of gaseous species. On the other hand, spatial discretization for gradients and for pressure of

gas phase are based on the least-squares cell method and PRESTO! method, respectively.

Moreover, since the kinetics of combustion chemical reactions is extremely fast, it is a good approximation to assume that there is no accumulation of intermediates during the combustion processes. This means that the rate of consumption of any reaction intermediate is approximately equal to its rate of formation. Under such circumstances, chemical species in the gas phase reach quickly steady-state concentrations, and the fluid phase may be modeled as a steady-state flow. As a matter of fact, only at the very beginning of the reaction one observes deviations from the steady-state approximation. This time interval corresponds to the time necessary by the gas phase to attain the steady state.

While the concentrations of the gaseous species may be considered constant during most of the time of the combustion process, the coal particles continue to change their trajectories due to the interactions with other particles and collisions with the walls of the vessel. In view of this, transient discrete element method simulations are coupled to the steady flow solution, where each particle of the solid–gas mixture is tracked every time that a particle iteration is performed. For this purpose, one performs 20 particle iterations for each 40 iterations of the continuous phase, such that the particle time step size is set equal to 0.5×10^{-3} s. Then, calculations proceed until a converged flow solution is obtained.

3.1 Analysis of the discrete element method simulation

Coal combustion is a complex process involving many parallel and consecutive reactions that are mainly governed by the interfacial transfer rates of mass and heat. Because coal presents a very complex chemical composition, it is difficult

Table 2 Chemical reactions employed in the simulation [5,15,18]

	Reaction	Pre-exponential factor	Activation energy (kJ mol ⁻¹)
Volatiles + $\frac{7}{4}$ O ₂ (g) \rightarrow CO ₂ (g) + $\frac{3}{2}$ H ₂ O (g)	1	$2.12 \times 10^{11} \text{L mol}^{-1} \text{s}^{-1}$	203
$C(s) + \frac{1}{2}O_2(g) \rightarrow CO(g)$	2	$52 \mathrm{g}\mathrm{m}^{-2}\mathrm{s}^{-1}$	61
$C(s) + CO_2(g) \rightarrow 2CO(g)$	3	$73 \mathrm{g} \mathrm{m}^{-2} \mathrm{s}^{-1}$	112
$C(s) + H_2O(g) \rightarrow H_2(g) + CO(g)$	4	$78 \mathrm{g}\mathrm{m}^{-2}\mathrm{s}^{-1}$	115
$H_2\left(g\right) + \frac{1}{2}O_2\left(g\right) \rightarrow H_2O\left(g\right)$	5	$2.23 \times 10^{12} L mol^{-1} s^{-1}$	167
$CO(g) + 1/2O_2(g) \rightarrow CO_2(g)$	6	$2.75 \times 10^7 L mol^{-1} s^{-1}$	84

The temperature exponent is assumed to be equal to zero for all chemical reactions

 Table 3
 Boundary conditions

 employed in the simulation

	Hydraulic diameter (m)	Turbulence intensity (%)	
Large air inlet	0.75	10	
Small air inlet	0.25	5	
Outlet	1.00	5	



Fig. 4 Chemical structure of medium-volatile coal, where R represents a radical. By depending on the source and the coal rank, the chemical structure of coal may be different

to establish a simple correlation between thermochemical parameters and the chemical structure through a traditional physicochemical model. For this reason, discrete element method simulations become a very important tool in the modeling of combustion chemical reactions since they permit to estimate thermochemical and kinetic data from physicochemical parameters of the chemical species.

In a simplistic view, coal is composed of a mixture of aromatic compounds, which are connected by an aliphatic chain (Fig. 4). When the system reaches high temperatures during the devolatization step, some chemical bonds in the structure of the coal start breaking, so that a mixture of solid, liquid, and gaseous substances is formed. Then, as coal is devolatized at a rate k_0^{dev} , the produced volatile species CO(g), CO₂(g), H₂O(g), H₂(g) *etc.* diffuse into the porous structure of coal

causing a swelling of the particles and a slight increase in the particle diameters (Fig. 5). Simultaneously with the increase in the diameter, coal particles experience in turn a decrease in their masses (Fig. 6) due to a conversion of coal into char (Fig. 7). Finally, in the next step the carbon atoms located on the char surface are partially oxidized by the molecules of $O_2(g)$, $CO_2(g)$, and $H_2O(g)$ present in the gas phase to essentially produce carbon monoxide and hydrogen (reactions 2–4), which, in turn, react with $O_2(g)$ to regenerate $CO_2(g)$ and $H_2O(g)$, according to reactions 5 and 6.

One can also analyze the kinetics of each chemical step previously mentioned from discrete element method simulations. Figures 8 and 9, respectively, show the rates for the volumetric reactions and the changes in the mass fraction of some chemical species that take part into the combustion process. Note that the contour graphs for the mass fraction of hydrogen and the rate of reaction 5 coincide. This indicates that $H_2(g)$ is the limiting reactant in reaction 5, and therefore, the amount of water formed is limited by the mass of $H_2(g)$. In addition, observe that in Figure 8 the reaction rate of reaction 5 is much smaller than the rate of reaction 6. This result is an immediate consequence of the high activation energy for reaction 5.

Figure 9 also provides information about the sequence of chemical steps that occur during the combustion of coal particles. As soon as the coal particles enter into the reaction chamber, they undergo the process of devolatization and gases are released into the gas phase. Such gases will immediately react with oxygen in the first half of the chamber to produce small amounts of $CO_2(g)$ and $H_2O(g)$, according to reaction 1. Just after the devolatization step, the char accumulated on the coal particles is burned out and CO(g) is released

Fig. 5 Changes observed in the parcel diameter during the first instants of the devolatization step

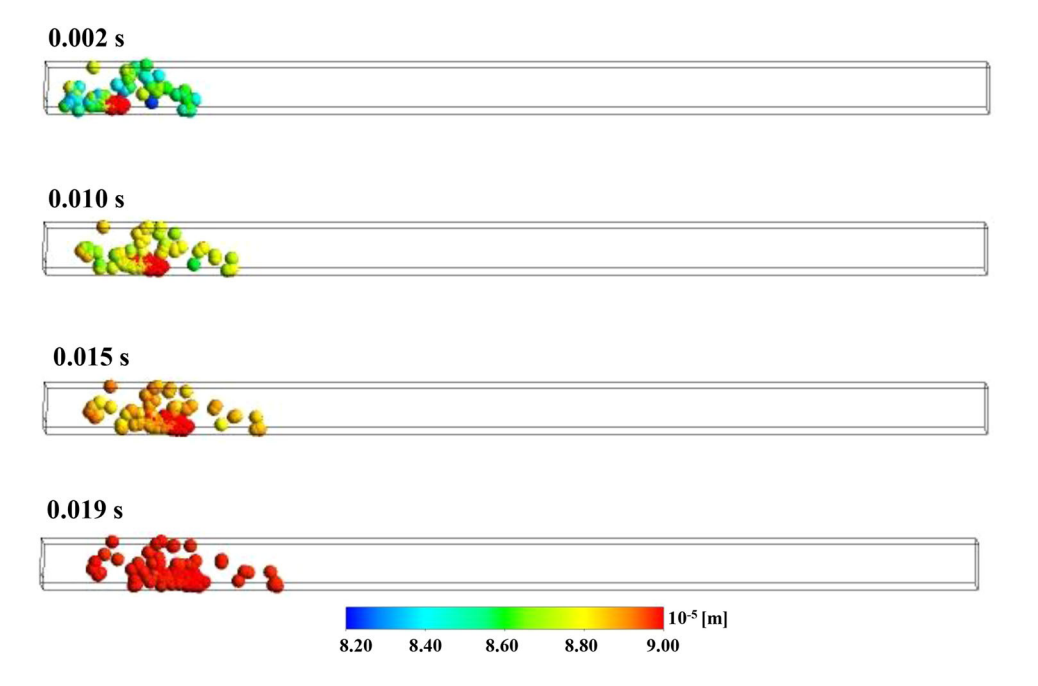
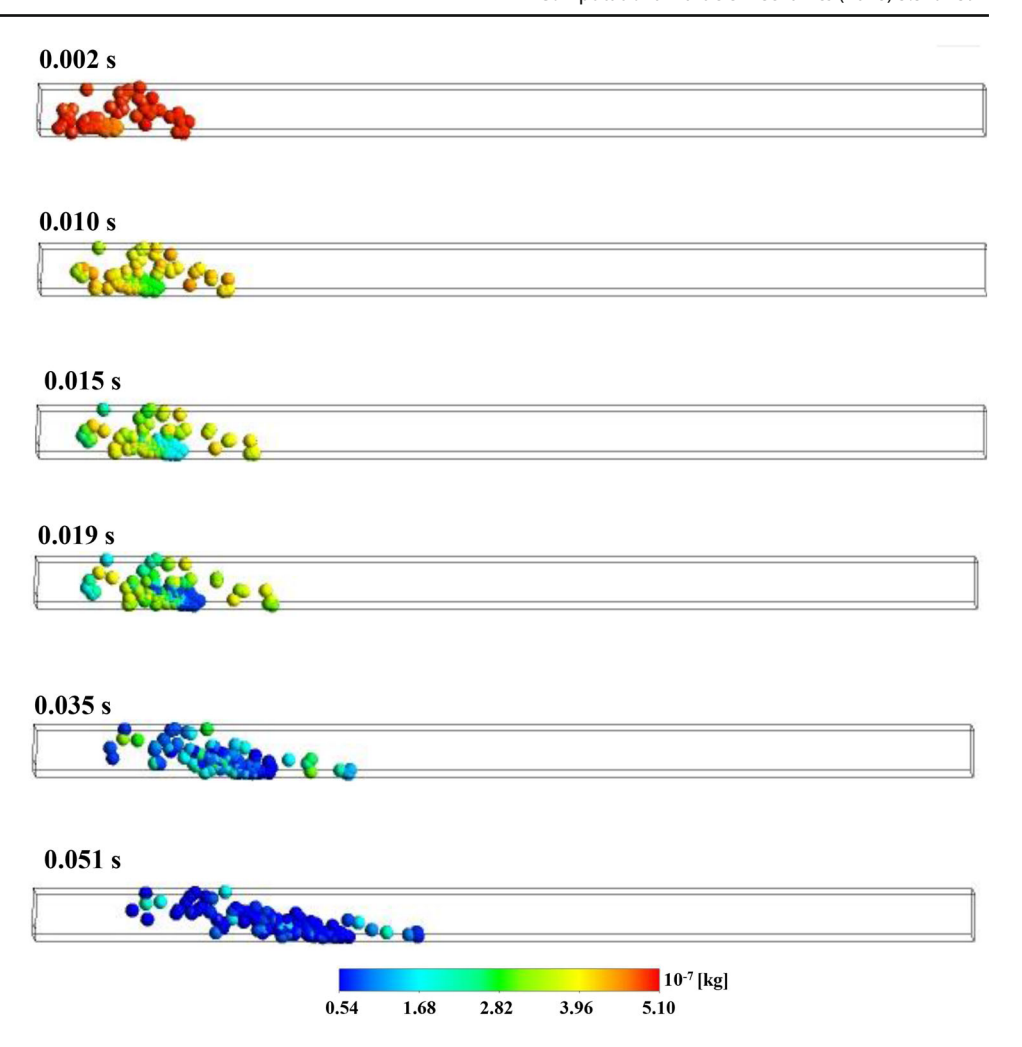




Fig. 6 Changes observed in the parcel mass during the first instants of the process of combustion



into the atmosphere, according to reactions 2–4. Then, next CO(g) and $H_2(g)$ are respectively oxidized to $H_2O(g)$ and $CO_2(g)$ (reactions 5 and 6) and their mass fractions decrease as $H_2O(g)$ and $CO_2(g)$ are produced.

All reactions considered in the simulation of the combustion of coal are highly exothermic, so that the conversion of reactants into products may be favored, whenever the system temperature increases. Figure 10 presents the enthalpy profile in the chamber, where combustion of coal particles occurs. According to Fig. 10, one verifies that the enthalpy is larger in the regions where the devolatization rate and char burnout rate are larger. In addition, one observes that the change in the system entropy is also larger in the regions of high burnout rate and high devolatization rate. Therefore, both enthalpy and entropy contribute to the spontaneity of the coal combustion under the considered conditions.

4 Concluding remarks

In this work, the combustion of coal particles in a hightemperature reaction chamber operating in the turbulent regime is modeled through 3D discrete element method (DEM) simulations. In order to take into account the interfacial transfers of mass, linear momentum, and thermal energy between coal particles and the gas mixture during the combustion process, it is assumed that particle dynamics may influence the flow solution through source terms, which are defined from the balance equations of each particle of the mixture. Moreover, by describing the turbulent mixing of chemical species in the system according to the eddy dissipation model, the influence of eddies present in the gas phase on the mass transport of reactants toward the coal particle surface and on the rate of volumetric reactions is considered.

Once material laws have been specified for all constitutive quantities of the solid–gas mixture, the balance equations for solid and liquid phases are alternately solved for the fields $\mathbf{v}_f(\mathbf{x},t)$, $\gamma_f(\mathbf{x},t)$, $\alpha_f(\mathbf{x},t)$, $m_i(t)$, $\mathbf{v}_i(t)$, $\theta_i(t)$, and $\alpha_f^v(\mathbf{x},t)$ until a converged solution for each phase is obtained. Thus, from the obtained values for certain thermochemical and kinetic parameters, phenomenological aspects of the combustion process are discussed and related to changes in the chemical structure of the coal.



Fig. 7 Changes observed in the char mass fraction of parcels during the first instants of the process of combustion. The rate of conversion of coal into char is approximately 17%

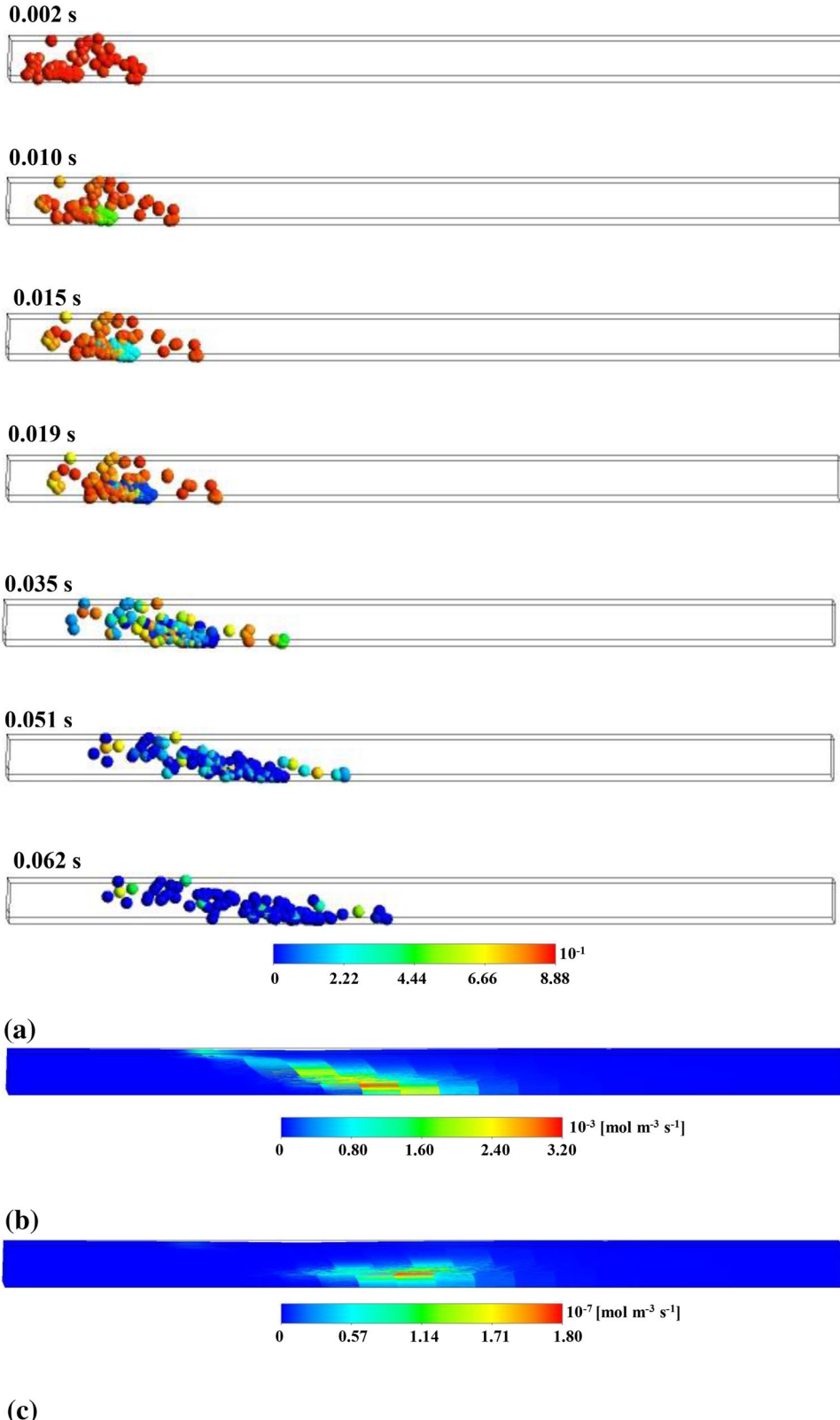


Fig. 8 Changes in the rates of the (a) reaction 1, (b) reaction 2, and (c) reaction 3 during the combustion process of coal particles. The contours correspond to average values obtained during the simulation

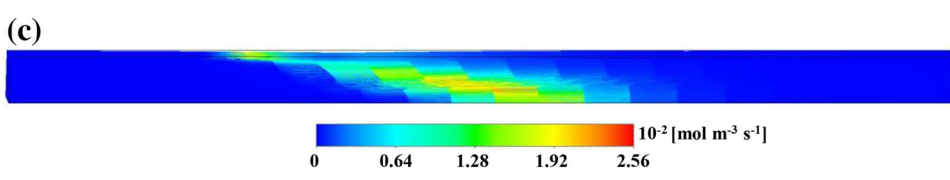




Fig. 9 Changes in the mass fractions of the chemical species during the combustion process of coal particles. The contours correspond to average values obtained during the simulation

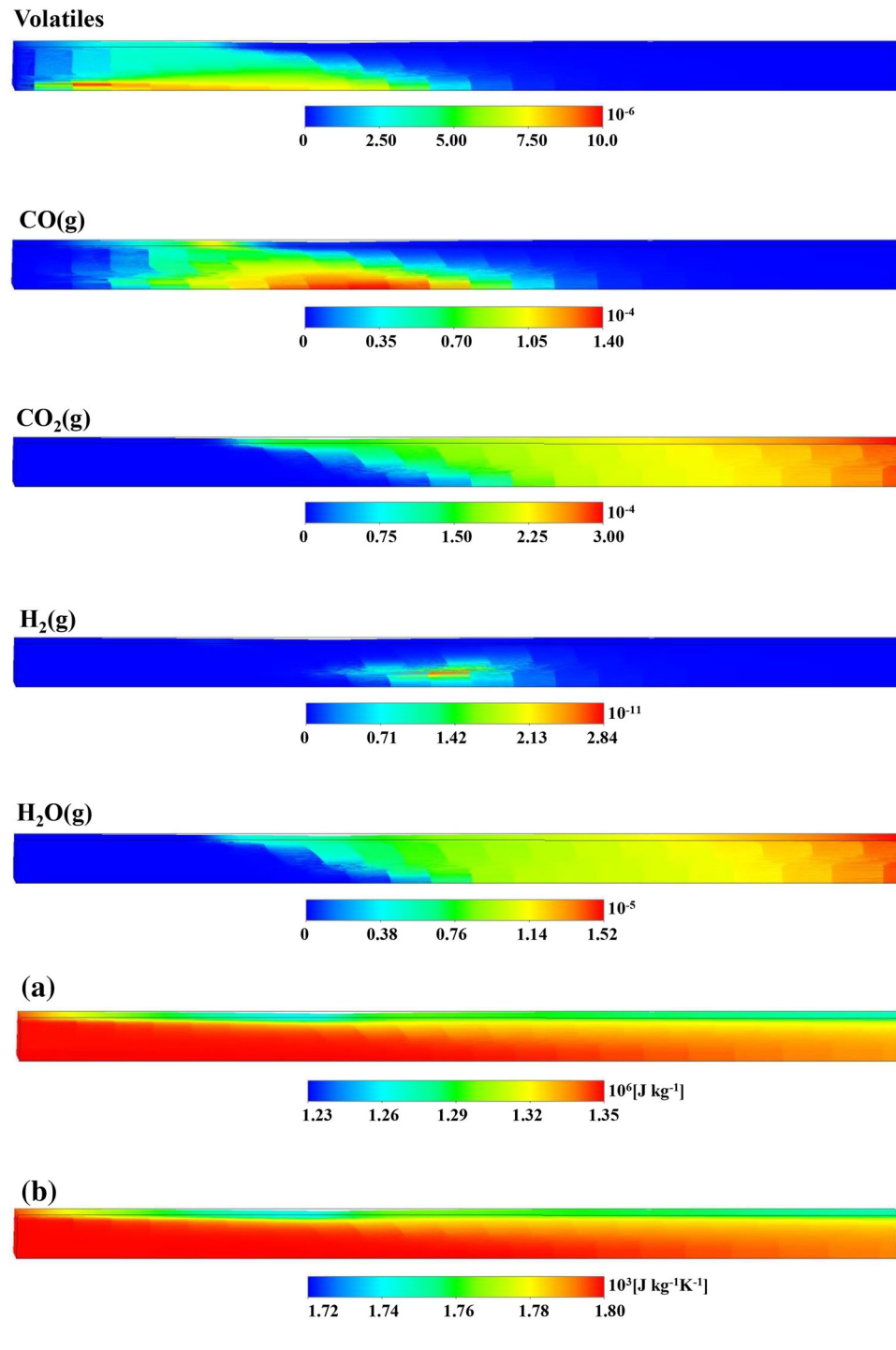
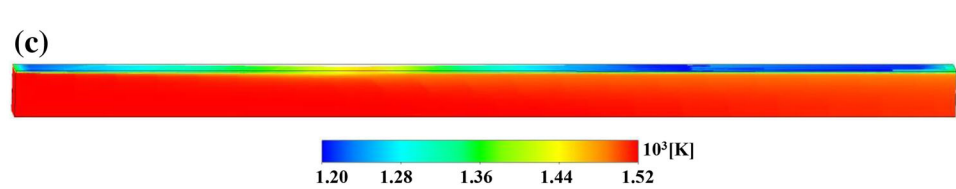


Fig. 10 Changes in the (a) enthalpy, (b) entropy, and (c) temperature of the system during the combustion process of coal particles. The contours correspond to average values obtained during the simulation





Although the results presented in this work are only related to the combustion process of coal particles, the described methodology may be employed to model other heterogeneous catalytic reactions and even a sequence of competitive and parallel surface chemical reactions. By performing discrete element method simulations for heterogeneous catalytic reactions, one may follow not only the changes in the physicochemical behavior of the gas phase, but also the dynamics of each solid particle of the gas—solid mixture. In addition, the approach employed in this manuscript permits the identification of how each chemical step of the combustion process may become a source of mass and energy for the gas phase.

Funding The first author acknowledges Brazilian Coordination for the Improvement of Higher Education Personnel (CAPES) and Alexander von Humboldt Stiftung for the financial support (Process BEX 8227/14-4).

Compliance with ethical standards

Conflict of interest The authors declare that they have no conflict of interest.

References

- Alobaid F, Ströhle J, Epple B (2013) Extended CFD/DEM model for the simulation of circulating fluidized bed. Adv Powder Technol 24:403–415
- 2. ANSYS Inc. (2012) Tutorial: multiple char reactions. Canonsburg
- 3. ANSYS Inc. (2015) ANSYS Fluent 16.2. Canonsburg
- ANSYS Inc. (2015) ANSYS fluent theory guide release 16.2. Canonsburg
- Badzioch S, Hawksley PGW (1970) Kinetics of thermal decomposition of pulverized coal particles. Ind Eng Chem Process Des Dev 9:521–530
- Boyd RK, Kent JH (1988) Three-dimensional furnace computer modeling. Symp (Int) Combust 21:265–274
- Bulíček M, Málek J, Rajagopal KR (2012) On Kelvin–Voigt model and its generalizations. Evol Equ Contr Theor 01:17–42

- Cundall PA, Strack OD (1979) A discrete numerical model for granular assemblies. Geotechnique 29:47–65
- Deen NG, van Sint Amaland M, van der Hoef MA, Kuipers JAM (2007) Review of discrete particle modeling of fluidized beds. Chem Eng Sci 62:28–44
- Fan L, Zhu C (2005) Principles of gas-solid flows. Cambridge Press, Cambridge
- Hayes RE, Kolaczkowski ST (1997) Introduction to catalytic combustion. Gordon and Breach Science Publishers, Amsterdam
- Hutter K, Jöhnk KJ (2004) Continuum methods of physical modeling: continuum mechanics, dimensional analysis, turbulence. Springer, Berlin
- Krugel-Emden H, Simsek E, Rickelt S, Wirtz S, Scherer V (2007) Review and extension of normal force models for the discrete element method. Powder Technol 11:157–173
- Kumar KV, Porkadi K, Rocha F (2008) Langmuir–Hinshelwood kinetics—a theoretical study. Catal Commun 9:82–84
- Lide DR (ed) (2009) CRC handbook of chemistry and physics, 89th edn. CRC Press, Boca Raton
- Magnussen BF (1981) On the structure of turbulence and a generalized eddy dissipation concept for chemical reaction in turbulent flow. American Institute of Aeronautics and Astronautics, Saint Louis
- Magnussen BF, Hjertager BH (1977) On mathematical modeling of turbulent combustion with special emphasis on sort formation and combustion. Symp (Int) Combust 16:719–729
- Manion JA, Huie RE, Levin RD, B DR Jr, Orkin VL, Tsang W, McGiven WS, Hudgens JW, Knyazev VD, Atkinson DB, Chai E, Tereza AM, Lin C, Allison T, Mallard WG, Westley F, Herron JT, Hampson RF, Frizzell DH (2015) NIST chemical kinetics database 17. National Institute of Standards and Technology, Gaithersburg
- O'Rourke PJ (1981) Collective drop effects on vaporizing liquid sprays. Princeton University Press, Princeton
- Readey DW (2016) Kinetics in materials science and engineering. CRC Press, Boca Raton
- Reis MC, Wang Y (2017) A two-fluid model for reactive dilute solid-liquid mixtures with phase changes. Continuum Mech Thermodyn 29:509–534
- Sommerfeld M, van Wachen B, Oliemans R (2008) Best practice guidelines for computational fluid dynamics of dispersed multiphase flows. ERCOFTAC, Bedford
- Somorjai GA, Li Y (2010) Introduction to surface chemistry and catalysis, 2nd edn. Wiley, Hoboken
- Warnatz J, Maas U, Dibble R (2006) Combustion: physical and chemical fundamentals, modeling and simulation, experiments, pollutant formation. Springer, Berlin

